Dynamics and Balance Control of the Reaction Mass Pendulum (RMP): A 3D Multibody Pendulum with Variable Body Inertia

Amit K. Sanyal
Mechanical and Aerospace Engineering
New Mexico State University
Las Cruces, NM 88011
Email: asanyal@nmsu.edu

Ambarish Goswami
Honda Research Institute US
Mountain View, California 94043
Email: agoswami@honda-ri.com

Pendulum models have been studied as benchmark problems for development of nonlinear control schemes, as well as reduced-order models for the dynamics analysis of gait, balance and fall for humanoid robots. We have earlier introduced the Reaction Mass Pendulum (RMP), an extension of the traditional inverted pendulum models, that explicitly captures the variable rotational inertia and angular momentum of a human or humanoid. The RMP consists of an extensible "leg", and a "body" with moving proof masses that gives rise to the variable rotational inertia. In this paper we present a thorough analysis of the RMP, which is treated as a 3D multibody system in its own right. We derive the complete kinematics and dynamics equations of the RMP system and obtain its equilibrium conditions. We show that the equilibria of this system consist of an unstable equilibrium manifold and a stable equilibrium manifold. Next we present a nonlinear control scheme for the RMP, which is an underactuated system with three unactuated degrees of freedom. This scheme asymptotically stabilizes this underactuated system at its unstable equilibrium manifold, with a vertically upright configuration for the "leg" of the RMP. The domain of convergence of this stabilization scheme is shown to be almost global in the state space of the RMP. Numerical simulation results verify this stability property of the control scheme and demonstrate its effectiveness in stabilizing the unstable equilibrium manifold.

1 Background and Motivation

Pendulum models have provided a rich source of examples in nonlinear dynamics and nonlinear control. They are useful for both pedagogical and research reasons. They represent physical mechanisms that can be analyzed as reduced-order or simplified versions of mechanical systems that arise in robotics and uninhabited vehicles. Control problems for planar and spherical pendulum models have been studied in [1–3] and various other sources. In this paper, we study the dynamics and control of a 3D multibody pendulum that has applications to reduced-order modeling of locomotion of humanoid robots.

Bipedal gait of humanoid robots is often modeled with various versions of the inverted pendulum model, such as the 2D and 3D linear inverted pendulums (LIP) [4, 5], the cart-table model [6], the variable impedance LIP [7], the spring-loaded inverted pendulum [8], and the angular momentum pendulum model (AMPM) [9,10]. These reduced order models have been very beneficial for the analysis and prediction of gait and balance [11]. The inverted pendulum models allow us to ignore the movements of the multitude of individual limbs and instead focus on two points of fundamental importance – the center of mass (CoM) and the center of pressure (CoP) – and the "lean line" joining them. A limitation of the above models (except [9, 10]) is that they represent the entire humanoid body only as a point mass and do not characterize the significant rotational inertia. Consequences of neglecting the rotational inertia is that the angular momentum of the system about its CoM must be zero and the ground reaction force (GRF), $\boldsymbol{f}$ must be directed along the lean line. Humanoid robots have no reason to obey these artificial conditions, and in general, they do not. It has been reported that during human gait, even at normal speed, $\boldsymbol{f}$ diverges from the lean line [12] and this may be important for maintaining balance. Fig. 1 schematically depicts this important difference between the traditional inverted pendulum models and a planar model that contains non-zero rotational inertia. The model with inertia captures the external centroidal moment (ECM), τ_e, created by the GRF about the CoM and is given

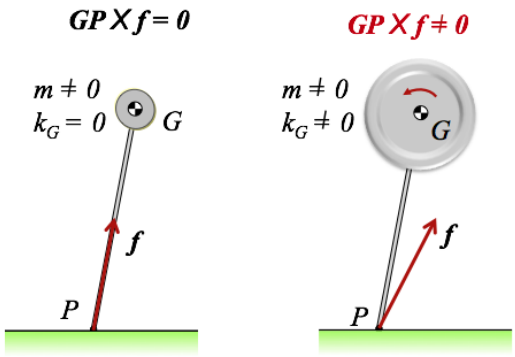

Fig. 1. This figure illustrates the main difference between the traditional point-mass inverted pendulum model with zero rotational inertia (left) and models containing non-zero rotational inertia (right). The point mass in the traditional pendulum model forces the ground reaction force, $\boldsymbol{f}$, to pass through the center of mass. A reaction mass type pendulum, by virtue of its non-zero rotational inertia, allows the ground reaction force to deviate from the lean line.

by $\boldsymbol{\tau_e} = \boldsymbol{GP} \times \boldsymbol{f}$. The rotational inertia and the associated angular momentum are important components of humanoid movement and especially of balance, as have been reported in [13, 14]. Direct manipulation of angular and linear momentum has been suggested as a reasonable, and sometimes preferable, way to control a robot [15–17]. Planar inverted pendulum models with variable length and inertia have also been considered in the book [18].

The Reaction Mass Pendulum (RMP) model [19] extends the existing inverted pendulum models by replacing the point mass at the top of the pendulum with an extended variable 3D inertia. The mass of the system remains unchanged but the model now has a non-zero variable rotational inertia in the form of the 3D reaction mass which characterizes the *instantaneous* aggregate rotational inertia of the system projected at its CoM. This paper generalizes the RMP model of [19] by introducing a massive leg with non-negligible inertia, and a body frame structure with non-negligible mass and variable inertia. The leg and body are connected by a ball joint which has passive damping. It then analyzes the dynamics of this generalized RMP as an underactuated, variable inertia, multibody system. It also obtains a control scheme for the RMP that asymptotically stabilizes "inverted" orientations of the RMP, with an almost global domain of convergence under certain actuation assumptions.

2 Conceptual Model of the RMP

In this section we present a full description of a conceptual model of the RMP model and briefly explain how the model can be derived from a given humanoid. The RMP consists of two main parts: a prismatic jointed "telescopic" (extensible) leg and a variable inertia body. The leg makes a unilateral contact with the ground or a flat surface through a ball joint (the "ankle joint") that is actuated. The variable inertia body is attached to the leg via a ball joint (the "hip joint"), which has passive (viscous) damping. For convenience in modeling the dynamics, we assume that the location of the hip joint coincides with the CoM of the RMP body. The variable inertia of the body captures the centroidal composite rigid body (CCRB) inertia of the robot, which is the instantaneous generalized inertia of the robot body about its CoM. The CCRB inertia is also called locked inertia in the field of geometric mechanics [20]. Additionally, the rotational motion of the body is such that the centroidal angular momentum of the RMP is instantaneously equal to that of the humanoid robot.

This conceptual model of the RMP provides a variable inertia matrix through the variable inertia of the RMP body, where the variation is attained by the movement of three pairs of proof masses that are linearly actuated along three orthogonal directions. These directions coincide with the principal axes of the CCRB inertia ellipsoid. Along each axis, the pair of point masses move in synchrony such that they are always equidistant from the mass center of the RMP body; thus, the mass center of the RMP body does not change as a result of the motion of the proof masses. The six point masses have equal mass, each having about one-sixth of the total mass of the upper body of the humanoid. At a given instant the distances between the masses on each axis depend on the rotational inertia of the robot about that axis. This representation of the RMP is shown in Fig. 2 and is used as the basis for a novel multibody system as described in this paper in detail.

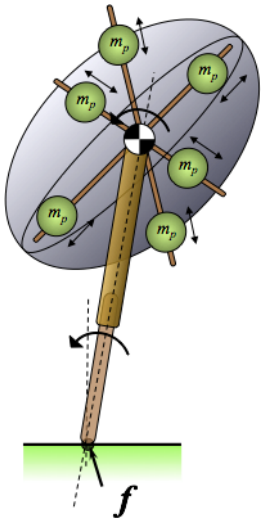

Fig. 2. Conceptual realization of the 3D RMP. The RMP consists of a telescopic leg connecting the CoP and CoM, and a rotating body. In 3D, the rotating ellipsoidal body is mechanically equivalent to six equal masses on three mutually perpendicular rotating tracks. The CoM of the RMP is fixed at the common mid point of the tracks. This is the point about which the tracks themselves can rotate.

With this model, the RMP can be categorized to the class of rigid body and multibody pendulum models that have appeared in prior publications [21–24]. An existing planar analog of the 3D RMP model is the reaction wheel (or inertia wheel) pendulum model, described in [25]; however, the reaction wheel pendulum does not have a variable body inertia in the plane.

3 Dynamics of the Reaction Mass Pendulum

In this section, we present the mathematical model of the dynamics of the reaction mass pendulum. The first appearance of a complete dynamics model of an underactuated RMP, with an actuated hip joint and no actuation of the ankle joint, was in [26]. Here we obtain a dynamics model, using variational mechanics, of the underactuated RMP with an actuated ankle joint and passive damping at the hip joint. We begin with a physical description of the RMP, followed by the equations of motion consisting of the kinematics and dynamics equations, and conclude this section with the equilibria of the RMP dynamics. This dynamics model is used subsequently for a nonlinear control design.

3.1 Physical Description

We consider the RMP model as a multibody system consisting of a prismatic jointed variable-length leg and three pairs of proof mass actuators (PMAs) moving pairwise along three mutually orthogonal directions. The motion of these three pairs of PMAs along the three mutually orthogonal tracks is such that their mass distribution is inertially equivalent to an ellipsoid of uniform mass density with major axes along these orthogonal tracks and with total mass equal to the total mass of the PMAs. We refer to this assembly of tracks with proof mass actuators as the "PMA assembly" hereon in this paper. For simplicity in analysis, we consider the CoM of the leg of the RMP to always coincide with the CoM of the reaction mass ellipsoid. Therefore this also locates the CoM of the RMP system, which simplifies the dynamic analysis of the motion of the RMP. Motion of the RMP in 3D Euclidean space consists of: (1) translational motion of the CoM at the tip of the variable-length leg; (2) rotational motion of the leg given by rotation and angular velocity of the leg about the CoM of the system; (3) rotational motion of the assembly of the PMAs about the CoM of the system; and (4) internal (shape) motion of the three pairs of PMAs along the three mutually orthogonal tracks.

3.2 Equations of Motion

Here we derive and provide the equations of motion of the RMP model, and obtain its equilibria.

3.2.1 Kinematics and Configuration Space

We introduce three coordinate frames to describe the configuration of the RMP. An inertial coordinate frame $\{\boldsymbol{I}\}$ is fixed to the ground with its origin at the CoP, where the ankle joint connects the RMP leg to the ground. A coordinate frame is fixed to the RMP's leg with its origin at the hip joint, which is also the CoM of the RMP body, and is denoted $\{\boldsymbol{L}\}$. Finally, we have an RMP body (PMA assembly) fixed coordinate frame $\{\boldsymbol{P}\}$ with its origin at the hip joint (CoM of body) and its axes aligned with the tracks of the PMAs. These coordinate frames along with associated configuration variables, are shown in Fig. 3. We next define the configuration variables of the RMP as follows:

$\rho \triangleq$ length of the leg of the RMP, which is also the distance between the CoM of body and the CoP,

$\boldsymbol{R}_L \triangleq$ rotation matrix from leg-fixed CoM frame $\{\boldsymbol{L}\}$ to inertial frame $\{\boldsymbol{I}\}$ fixed at CoP,

$\boldsymbol{R}_{PL} \triangleq$ rotation matrix from PMA assembly-fixed CoM frame $\{\boldsymbol{P}\}$ to leg-fixed CoM frame $\{\boldsymbol{L}\}$,

$\boldsymbol{s} \triangleq [s_1 \;\; s_2 \;\; s_3]^{\mathrm{T}} =$ vector of locations of the three pairs of proof mass actuators in the PMA assembly-fixed CoM frame $\{\boldsymbol{P}\}$.

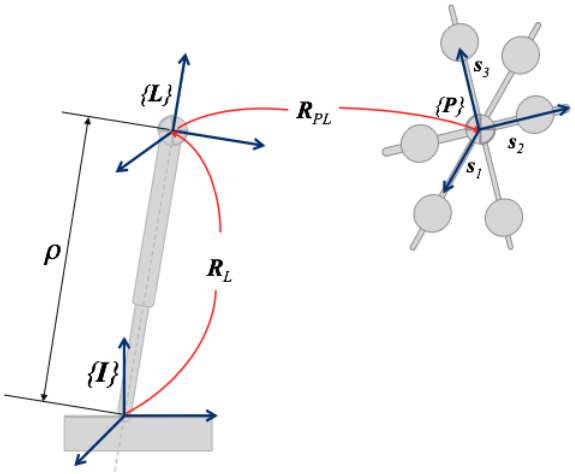

Fig. 3. Three coordinate frames are used to describe the RMP kinematics: the CoP-fixed inertial frame $\{\boldsymbol{I}\}$, the leg-fixed frame $\{\boldsymbol{L}\}$ located at the CoM and aligned with the leg axis, and the PMA assembly-fixed frame $\{\boldsymbol{P}\}$ located at the CoM. ρ is the length of the RMP leg, $\boldsymbol{R}_L$ is the rotation matrix from $\{\boldsymbol{L}\}$ to $\{\boldsymbol{I}\}$, $\boldsymbol{R}_{PL}$ is the rotation matrix from $\{\boldsymbol{P}\}$ to $\{\boldsymbol{L}\}$, and $\boldsymbol{s} = [s_1 \;\; s_2 \;\; s_3]^{\mathrm{T}}$ is the vector of locations of the three pairs of proof mass actuators in $\{\boldsymbol{P}\}$.

The vector $\boldsymbol{s}$ of PMA locations is in a compact subspace $\mathcal{S}$ of $\mathbb{R}^3$ and the scalar length ρ of the RMP leg be in a bounded interval $[0, r]$ of $\mathbb{R}$. The configuration space of the RMP is therefore $\mathcal{C} = [0, r] \times \mathrm{SO}(3) \times \mathrm{SO}(3) \times \mathcal{S}$, which is ten dimensional, corresponding to the ten degrees of freedom (DOFs) of this RMP model. These DOFs are: one DOF corresponding to the scalar leg length ρ, three DOFs for the attitude of the leg $\boldsymbol{R}_L$, three DOFs for the attitude of the PMA assembly $\boldsymbol{R}_{PL}$, and three DOFs for the vector s of PMA locations. The inertial coordinate frame is defined such that its third axis is along the direction of the uniform gravity force. Let $\boldsymbol{e}_i$ denote the ith column vector of the 3×3 identity matrix. Therefore $g\boldsymbol{e}_3$ is the inertial acceleration vector due to uniform gravity, where g is its magnitude.

If the RMP leg-fixed coordinate frame has its third coordinate axis along the longitudinal axis of the leg, the position of the CoM in the CoP-fixed inertial frame is $\boldsymbol{b} = \rho \boldsymbol{R}_L \boldsymbol{e}_3$. Let ν denote the translational velocity of the CoM with respect to inertia frame $\{\boldsymbol{I}\}$ and represent in the leg-fixed CoM frame $\{\boldsymbol{L}\}$, and let $\boldsymbol{\Omega}_L$ be the angular velocity of the RMP leg represented in the leg-fixed CoM frame $\{\boldsymbol{L}\}$. Let $\boldsymbol{\Omega}_{PL}$ denote the angular velocity of the PMA assembly with respect to the RMP leg and represented in the RMP body frame $\{\boldsymbol{P}\}$. The kinematics for rotational motion of the leg about the CoM,

rotational motion of the PMA assembly with respect to the RMP leg, and the translational motion of the CoM with respect to the CoP, are given by:

$$\dot{\boldsymbol{R}}_L = \boldsymbol{R}_L \boldsymbol{\Omega}_L{}^{\times} \tag{1}$$

$$\dot{\boldsymbol{R}}_{PL} = \boldsymbol{R}_{PL} \boldsymbol{\Omega}_{PL}{}^{\times} \tag{2}$$

$$\boldsymbol{\nu} = \boldsymbol{R}_L{}^{\mathrm{T}} \dot{b} = \dot{\rho}\, \boldsymbol{e}_3 + \rho \boldsymbol{\Omega}_L \times \boldsymbol{e}_3 \tag{3}$$

where $\boldsymbol{\Omega}^{\times}$ is the skew-symmetric cross-product matrix defined by $\boldsymbol{\Omega}^{\times}\boldsymbol{\nu} = \boldsymbol{\Omega} \times \boldsymbol{\nu}$.

Therefore, the attitude of the PMA assembly with respect to the CoP-fixed inertial frame is $\boldsymbol{R}_P = \boldsymbol{R}_L \boldsymbol{R}_{PL}$. The corresponding angular velocity of the PMA assembly with respect to the inertial frame is obtained from time derivative of $\boldsymbol{R}_P$ as

$$\dot{\boldsymbol{R}}_P = \boldsymbol{R}_P \boldsymbol{\Omega}_P{}^{\times} \text{ where } \boldsymbol{\Omega}_P = \boldsymbol{\Omega}_{PL} + \boldsymbol{R}_{PL}{}^{\mathrm{T}} \boldsymbol{\Omega}_L. \tag{4}$$

Hence, the position vectors of the PMAs of the ith pair in the CoP-fixed inertial coordinate frame are $\boldsymbol{b} \pm \boldsymbol{R}_P \boldsymbol{s}_i \boldsymbol{e}_i$, for $i = 1, 2, 3$. The velocities of the proof masses in the ith proof mass pair are therefore given by

$$\boldsymbol{\nu}_{i+} = \dot{\boldsymbol{b}} + \boldsymbol{R}_P(\dot{\boldsymbol{s}}_i \boldsymbol{e}_i + \boldsymbol{s}_i \boldsymbol{\Omega}_P \times \boldsymbol{e}_i),$$
$$\boldsymbol{\nu}_{i-} = \dot{\boldsymbol{b}} - \boldsymbol{R}_P(\dot{\boldsymbol{s}}_i \boldsymbol{e}_i + \boldsymbol{s}_i \boldsymbol{\Omega}_P \times \boldsymbol{e}_i),$$

where $\dot{\boldsymbol{b}} = \boldsymbol{R}_L \boldsymbol{\nu}$ is as given by equation (3).

3.2.2 Dynamics of RMP

The dynamics of the three-dimensional RMP consists of the translational and rotational dynamics about its CoM and the dynamics of its internal states. Let m_p denote the mass of each PMA (the six PMAs have equal masses) and let $\boldsymbol{J}_{P_0}$ denote the inertia tensor of the PMA frame minus the proof mass actuators about the CoM. Let m_L denote the mass and $\boldsymbol{J}_{L_0}$ denote the inertia tensor about the CoM of the leg of the RMP, so that the total mass of the RMP is $m = 6m_p + m_L$. The total kinetic energy of the PMA assembly is therefore given by

$$T_P = \sum_{i=1}^{3} m_p \left(\boldsymbol{\nu}^{\mathrm{T}} \boldsymbol{\nu} + \dot{s}_i^2 \right) + \frac{1}{2} \boldsymbol{\Omega}_P{}^{\mathrm{T}} \left(\boldsymbol{J}_{P_0} + \boldsymbol{K}_P(s) \right) \boldsymbol{\Omega}_P, \tag{5}$$

where

$$\boldsymbol{K}_P(s) = -2 \sum_{i=1}^{3} m_p s_i^2 (\boldsymbol{e}_i{}^{\times})^2 \text{ and } \boldsymbol{\nu}^{\mathrm{T}} \boldsymbol{\nu} = \dot{\rho}^2 - \rho^2 \boldsymbol{\Omega}_L{}^{\mathrm{T}} (\boldsymbol{e}_3{}^{\times})^2 \boldsymbol{\Omega}_L.$$

The kinetic energy of the RMP leg is given by

$$T_L = \frac{1}{2} m_L \dot{\rho}^2 + \frac{1}{2} \boldsymbol{\Omega}_L{}^{\mathrm{T}} \left(\boldsymbol{J}_{L_0} - m_L \rho^2 (\boldsymbol{e}_3{}^{\times})^2 \right) \boldsymbol{\Omega}_L. \tag{6}$$

Denote by $\boldsymbol{\Gamma}_L = \boldsymbol{R}_L{}^{\mathrm{T}} \boldsymbol{e}_3$ the direction of gravity expressed in the leg-fixed coordinate frame; note that $\boldsymbol{e}_3 = [0\ 0\ 1]^{\mathrm{T}}$ denotes the direction of gravity in the inertial frame. The total potential energy of the RMP system is given by

$$V = -mg\rho \boldsymbol{e}_3{}^{\mathrm{T}} \boldsymbol{R}_L{}^{\mathrm{T}} \boldsymbol{e}_3 = -mg\rho \boldsymbol{e}_3{}^{\mathrm{T}} \boldsymbol{\Gamma}_L. \tag{7}$$

Therefore the Lagrangian of the RMP is given by

$$\begin{aligned} \mathcal{L} =& T_P + T_L - V \\ =& \frac{1}{2} m \dot{\rho}^2 + \frac{1}{2} \boldsymbol{\Omega}_L{}^{\mathrm{T}} \boldsymbol{J}_L(\rho) \boldsymbol{\Omega}_L + \frac{1}{2} \boldsymbol{\Omega}_P{}^{\mathrm{T}} \boldsymbol{J}_P(s) \boldsymbol{\Omega}_P \\ &+ m_p \dot{\boldsymbol{s}}^{\mathrm{T}} \dot{\boldsymbol{s}} + mg\rho \boldsymbol{e}_3{}^{\mathrm{T}} \boldsymbol{\Gamma}_L \end{aligned} \tag{8}$$

where $\boldsymbol{K}_L(\rho) = -m\rho^2 \left(\boldsymbol{e}_3{}^{\times} \right)^2$, $\boldsymbol{J}_L(\rho) = \boldsymbol{J}_{L_0} + \boldsymbol{K}_L$ and $\boldsymbol{J}_P(\boldsymbol{s}) = \boldsymbol{J}_{P_0} + \boldsymbol{K}_P(\boldsymbol{s})$. $\boldsymbol{K}_P(\boldsymbol{s})$ and $\boldsymbol{K}_L(\rho)$ are shape-dependent inertia terms. $\boldsymbol{K}_P$ accounts for the portion of the inertia of the PMA assembly that varies with $\boldsymbol{s}$. $\boldsymbol{K}_L$, on the other hand, varies with the leg length of the RMP.

In (8), $\boldsymbol{\Omega}_P$ is dependent on $\boldsymbol{\Omega}_L$, $\boldsymbol{R}_{PL}$ and $\boldsymbol{\Omega}_{PL}$ as given by (4). The following result gives the dynamics equations of motion for the RMP system.

Proposition 1. *Let f_L be the force applied by the prismatic actuator along the leg of the reaction mass pendulum in the inertial frame, $\boldsymbol{\tau}_L$ denote the control torque vector applied to the leg at the contact point (CoP), and $\boldsymbol{u}_s$ be the vector of control forces applied to the proof mass actuators in the PMA-fixed coordinate frame. Let $\boldsymbol{\tau}_D = -\boldsymbol{D}\boldsymbol{\Omega}_{PL}$, where $\boldsymbol{D}$ is a positive definite matrix, be the torque due to viscous damping at the spherical "hip joint" that attaches the proof mass assembly to the leg, expressed in the $\{\boldsymbol{P}\}$ frame. The dynamics of the reaction mass pendulum model are then given by the following equations*

$$m\ddot{\rho} = -m\rho \boldsymbol{\Omega}_L{}^{\mathrm{T}} \left(\boldsymbol{e}_3{}^{\times} \right)^2 \boldsymbol{\Omega}_L + mg \boldsymbol{e}_3{}^{\mathrm{T}} \boldsymbol{\Gamma}_L + f_L, \tag{9}$$

$$\begin{aligned} \boldsymbol{J}_L(\rho) \dot{\boldsymbol{\Omega}}_L =& \boldsymbol{J}_L(\rho) \boldsymbol{\Omega}_L \times \boldsymbol{\Omega}_L + 2m\rho\dot{\rho} \left(\boldsymbol{e}_3{}^{\times} \right)^2 \boldsymbol{\Omega}_L + mg\rho \boldsymbol{e}_3 \times \boldsymbol{\Gamma}_L \\ &- \boldsymbol{R}_{PL} \boldsymbol{\tau}_D + \boldsymbol{\tau}_L, \end{aligned} \tag{10}$$

$$\boldsymbol{J}_P(\boldsymbol{s}) \dot{\boldsymbol{\Omega}}_P = \boldsymbol{J}_P(\boldsymbol{s}) \boldsymbol{\Omega}_P \times \boldsymbol{\Omega}_P - \boldsymbol{N}(\boldsymbol{s}, \dot{\boldsymbol{s}}) \boldsymbol{\Omega}_P + \boldsymbol{\tau}_D, \tag{11}$$

$$2m_p \ddot{\boldsymbol{s}} = \boldsymbol{L}(\boldsymbol{s}, \boldsymbol{\Omega}_P) + \boldsymbol{u}_s, \tag{12}$$

where $\boldsymbol{N}(\boldsymbol{s}, \dot{\boldsymbol{s}}) = \dfrac{\mathrm{d}}{\mathrm{d}t} \boldsymbol{K}_P(\boldsymbol{s})$

$$= 4m_p \operatorname{diag}\{s_2\dot{s}_2 + s_3\dot{s}_3, s_1\dot{s}_1 + s_3\dot{s}_3, s_1\dot{s}_1 + s_2\dot{s}_2\},$$

and $\boldsymbol{L}(\boldsymbol{s}, \boldsymbol{\Omega}_P) = \dfrac{\partial}{\partial \boldsymbol{s}} \left(\frac{1}{2} \boldsymbol{\Omega}_P{}^{\mathrm{T}} \boldsymbol{K}_P \boldsymbol{\Omega}_P \right) = 2m_p \begin{bmatrix} s_1(\Omega_{P_2}^2 + \Omega_{P_3}^2) \\ s_2(\Omega_{P_3}^2 + \Omega_{P_1}^2) \\ s_3(\Omega_{P_1}^2 + \Omega_{P_2}^2) \end{bmatrix}.$

Proof: The dynamics equations (9)-(12) are obtained by generalizing and applying the Lagrange-d'Alembert principle [27] to the nonlinear configuration space $\mathcal{C}$. Variations of the state variables ($\boldsymbol{R}_L$ and $\boldsymbol{R}_{PL}$) in SO(3) are in the form of *reduced variations* [28, 29], as follows:

$$\delta \boldsymbol{R}_L = \boldsymbol{R}_L \boldsymbol{\Sigma}_L^{\times}, \ \ \delta \boldsymbol{R}_{PL} = \boldsymbol{R}_{PL} \boldsymbol{\Sigma}_{PL}^{\times}, \tag{13}$$

where $\boldsymbol{\Sigma}_L, \boldsymbol{\Sigma}_{PL} \in \mathbb{R}^3$ describe variations tangent to SO(3). In addition, reduced variations of the angular velocities $\boldsymbol{\Omega}_L$ and $\boldsymbol{\Omega}_{PL}$ are given by [28, 29]:

$$\delta\boldsymbol{\Omega}_L = \dot{\boldsymbol{\Sigma}}_L + \boldsymbol{\Omega}_L \times \boldsymbol{\Sigma}_L, \;\; \delta\boldsymbol{\Omega}_{PL} = \dot{\boldsymbol{\Sigma}}_{PL} + \boldsymbol{\Omega}_{PL} \times \boldsymbol{\Sigma}_{PL}, \qquad (14)$$

where $\dot{\boldsymbol{\Sigma}}_L$ and $\dot{\boldsymbol{\Sigma}}_{PL}$ denote the time derivatives of $\boldsymbol{\Sigma}_L$ and $\boldsymbol{\Sigma}_{PL}$ respectively. The Lagrange-d'Alembert principle applied to the RMPsystem then takes the form

$$\int_{t_0}^{t_f} \left(\delta\mathcal{L} + \boldsymbol{\tau}_D^{\mathrm{T}} \boldsymbol{\Sigma}_{PL} + \boldsymbol{\tau}_L^{\mathrm{T}} \boldsymbol{\Sigma}_L + f_L \delta\rho + \boldsymbol{u}_s^{\mathrm{T}} \delta\boldsymbol{s} \right) \mathrm{d}t = 0, \qquad (15)$$

where $\delta\mathcal{L}$ denotes the first variation of the Lagrangian $\mathcal{L}$ with respect to all the state variables it depends on, and we define the inner product of two 3×3 matrices by $\langle A, B \rangle = \frac{1}{2}\mathrm{trace}(A^{\mathrm{T}}B)$. Eqn. (15) holds for any time interval $[t_0, t_f]$ over which the dynamics evolves. The first variation of the Lagrangian can be expressed as the sum of its first variation with respect to each of the state variables. Taking all terms in equation (15) dependent on $\delta\rho$ and $\delta\dot{\rho}$, we get:

$$\int_{t_0}^{t_f} \Big(m\dot{\rho}\delta\dot{\rho} - m\rho {\boldsymbol{\Omega}_L}^{\mathrm{T}} \left(\boldsymbol{e}_3^{\times}\right)^3 \boldsymbol{\Omega}_L \delta\rho + mg\boldsymbol{e}_3^{\mathrm{T}} \Gamma_L \delta\rho + \boldsymbol{f}_L \delta\rho \Big) \mathrm{d}t = 0,$$

which gives the dynamics equation (9) on integrating by parts. Collecting all terms in (15) dependent on $\boldsymbol{\Sigma}_L$ and $\delta\boldsymbol{\Omega}_L$, we get:

$$\int_{t_0}^{t_f} \delta{\boldsymbol{\Omega}_L}^{\mathrm{T}} \left[\boldsymbol{J}_L(\rho)\boldsymbol{\Omega}_L + \boldsymbol{R}_{PL}\boldsymbol{J}_P(\boldsymbol{s})(\boldsymbol{\Omega}_{PL} + {\boldsymbol{R}_{PL}}^{\mathrm{T}}\boldsymbol{\Omega}_L) \right] \mathrm{d}t + \int_{t_0}^{t_f} \left(mg\rho {\boldsymbol{e}_3}^{\mathrm{T}} (\boldsymbol{\Gamma}_L \times \boldsymbol{\Sigma}_L) + \boldsymbol{\tau}_L^{\mathrm{T}} \boldsymbol{\Sigma}_L \right) \mathrm{d}t = 0.$$

After substituting $\delta\boldsymbol{\Omega}_L$ in terms of $\boldsymbol{\Sigma}_L$ and its time derivative using equation (14), we can express these terms as:

$$\int_{t_0}^{t_f} \left(\ddot{\boldsymbol{\Sigma}}_L^{\mathrm{T}} - \boldsymbol{\Sigma}_L^{\mathrm{T}} {\boldsymbol{\Omega}_L}^{\times} \right) \left[\boldsymbol{J}_L(\rho)\boldsymbol{\Omega}_L + \boldsymbol{R}_{PL}\boldsymbol{J}_P(\boldsymbol{s})(\boldsymbol{\Omega}_{PL} + {\boldsymbol{R}_{PL}}^{\mathrm{T}}\boldsymbol{\Omega}_L) \right] \mathrm{d}t + \int_{t_0}^{t_f} \boldsymbol{\Sigma}_L^{\mathrm{T}} \left(mg\rho(\boldsymbol{e}_3 \times \boldsymbol{\Gamma}_L) + \boldsymbol{\tau}_L \right) \mathrm{d}t = 0.$$

After integration by parts, the above expression leads to the following equation of motion:

$$\frac{\mathrm{d}}{\mathrm{d}t}\left[\boldsymbol{J}_L(\rho)\boldsymbol{\Omega}_L + \boldsymbol{R}_{PL}\boldsymbol{J}_P(\boldsymbol{s})\boldsymbol{\Omega}_P \right] = \left[\boldsymbol{J}_L(\rho)\boldsymbol{\Omega}_L + \boldsymbol{R}_{PL}\boldsymbol{J}_P(\boldsymbol{s})\boldsymbol{\Omega}_P \right] \times \boldsymbol{\Omega}_L + mg\rho\boldsymbol{e}_3 \times \boldsymbol{\Gamma}_L + \boldsymbol{\tau}_L. \qquad (16)$$

Collecting all terms in (15) dependent on $\boldsymbol{\Sigma}_{PL}$ and $\delta\boldsymbol{\Omega}_{PL}$, we get:

$$\int_{t_0}^{t_f} \left(\delta{\boldsymbol{\Omega}_{PL}}^{\mathrm{T}} + {\boldsymbol{\Omega}_L}^{\mathrm{T}} \boldsymbol{R}_{PL} \boldsymbol{\Sigma}_{PL}^{\times} \right) \boldsymbol{J}_P (\boldsymbol{\Omega}_{PL} + {\boldsymbol{R}_{PL}}^{\mathrm{T}} \boldsymbol{\Omega}_L) \mathrm{d}t + \int_{t_0}^{t_f} \left(\boldsymbol{\Sigma}_{PL}^{\mathrm{T}} \boldsymbol{\tau}_D \right) \mathrm{d}t = 0.$$

Now substituting for $\delta\boldsymbol{\Omega}_{PL}$ in terms of $\boldsymbol{\Sigma}_{PL}$ and $\dot{\boldsymbol{\Sigma}}_{PL}$ using equation (14), we can rewrite the above expression as:

$$\int_{t_0}^{t_f} \left((\dot{\boldsymbol{\Sigma}}_{PL}^{\mathrm{T}} - \boldsymbol{\Sigma}_{PL}^{\mathrm{T}} {\boldsymbol{\Omega}_{PL}}^{\times}) \boldsymbol{J}_P \boldsymbol{\Omega}_P + \boldsymbol{\Sigma}_{PL}^{\mathrm{T}} \boldsymbol{\tau}_D \right) \mathrm{d}t = 0,$$

which gives, on integration by parts,

$$\frac{\mathrm{d}}{\mathrm{d}t}\left[\boldsymbol{J}_P(\boldsymbol{s})\boldsymbol{\Omega}_P \right] = \boldsymbol{J}_P(s)\boldsymbol{\Omega}_P \times \boldsymbol{\Omega}_P + \boldsymbol{\tau}_D, \qquad (17)$$

which is equivalent to dynamics equation (11). Finally, substituting equation (17) into equation (16), we get

$$\frac{\mathrm{d}}{\mathrm{d}t}\left[\boldsymbol{J}_L(\rho)\boldsymbol{\Omega}_L \right] + \boldsymbol{R}_{PL}\left[\boldsymbol{J}_P(\boldsymbol{s})\boldsymbol{\Omega}_P \times {\boldsymbol{R}_{PL}}^{\mathrm{T}}\boldsymbol{\Omega}_L \right] = \boldsymbol{J}_L(\rho)\boldsymbol{\Omega}_L \times \boldsymbol{\Omega}_L + \left(\boldsymbol{R}_{PL}\boldsymbol{J}_P(\boldsymbol{s})\boldsymbol{\Omega}_P \right) \times \boldsymbol{\Omega}_L + mg\rho\boldsymbol{e}_3 \times \boldsymbol{\Gamma}_L - \boldsymbol{R}_{PL}\boldsymbol{\tau}_D + \boldsymbol{\tau}_L.$$

Using the identity $\boldsymbol{R}\boldsymbol{v}^{\times}\boldsymbol{R}^{\mathrm{T}} = (\boldsymbol{R}\boldsymbol{v})^{\times}$ for $\boldsymbol{R} \in \mathrm{SO}(3)$ and $\boldsymbol{v} \in \mathbb{R}^3$, we can simplify the above expression to:

$$\frac{\mathrm{d}}{\mathrm{d}t}\left[\boldsymbol{J}_L(\rho)\boldsymbol{\Omega}_L \right] = \boldsymbol{J}_L(\rho)\boldsymbol{\Omega}_L \times \boldsymbol{\Omega}_L + mg\rho\boldsymbol{e}_3 \times \boldsymbol{\Gamma}_L - \boldsymbol{R}_{PL}\boldsymbol{\tau}_D + \boldsymbol{\tau}_L, \qquad (18)$$

which is equivalent to the attitude dynamics equation (10) for the RMP leg. The remaining equation of motion for the proof mass actuators is obtained by accounting for terms dependent on δs and $\delta\dot{s}$ in equation (15). These terms give us:

$$\int_{t_0}^{t_f} \left(2m_p \delta\dot{\boldsymbol{s}}^{\mathrm{T}} \dot{\boldsymbol{s}} + \delta\boldsymbol{s}^{\mathrm{T}} \boldsymbol{L}(\boldsymbol{s}, \boldsymbol{\Omega}_P) + \delta\boldsymbol{s}^{\mathrm{T}} \boldsymbol{u}_s \right) \mathrm{d}t = 0,$$

which gives the dynamics equation (12) on integration by parts. This completes the proof of Proposition 1. □

Note that these dynamics equations conform to the general form of the dynamics of an underactuated multibody system in uniform gravity, as given in [30]. Also note that equations (9)-(12) depend only on $\boldsymbol{\Gamma}_L = \boldsymbol{R}_L^{\mathrm{T}}\boldsymbol{e}_3$ and not on the full attitude $\boldsymbol{R}_L$ of the leg. This means that the dynamics is independent of instantaneous rotations about the direction of uniform gravity. In other words, the equations of motion do not change if the inertial coordinate frame is rotated by an arbitrary angle about its z-axis, which represents the direction of uniform gravity. This is expected for a rigid body or

multibody system in uniform gravity. We also note that the shape and attitude dynamics of the PMA assembly, given by equations (11)-(12) are directly coupled, and the attitude and shape (leg length) dynamics of the leg of the RMP, given by equations (9)-(10) are directly coupled. However, the only coupling between the dynamics of the RMP leg and that of the PMA assembly is through the torque $\boldsymbol{\tau}_P$ applied at the spherical joint connecting them. This is because the shape change of the PMA assembly is always "symmetric" about the center of mass, and therefore the CoM location is not varied by the symmetric movements of the three pairs of PMAs. This has important consequences in the design of control schemes for this system, as we show later. Finally, one can use the same set of dynamics equations for any other damping model for the hip joint besides the viscous damping model mentioned in the statement of Proposition 1.

Remark: The ankle joint of the RMP is modeled here as a spherical joint with three degrees of rotational freedom. However, in humanoid robots, the ankle joint has only two degrees of rotational freedom. In this case, the rotation of the leg about its longitudinal axis is not permitted. The RMP model given here can also be applied to the situation where rotation of the leg about its longitudinal axis is not permitted. In this case, the expression for $\boldsymbol{\Omega}_L$ in equation (10) would be of the form

$$\boldsymbol{\Omega}_L = \dot{\beta}\boldsymbol{e}_2 + \dot{\alpha}(\cos\beta\boldsymbol{e}_1 + \sin\beta\boldsymbol{e}_3),$$

where α and β are successive rotation angles about the leg's first and second axes in the $\{\boldsymbol{L}\}$ frame. Furthermore, in this case the third component of the leg torque vector, $\boldsymbol{\tau}_L$ in equation (10), will be a constraint torque that ensures that the third component of $\dot{\boldsymbol{\Omega}}_L$ is zero. The first two components of $\boldsymbol{\tau}_L$ would be control input torques that correspond to the degrees of freedom given by the rotation angles α and β of the spherical ankle joint.

3.2.3 Equilibria of the RMP Dynamics

The conditions for equilibria of the RMP dynamics are obtained from the dynamics equations (9)-(12) and kinematics equations (1)-(3) by setting $\dot{\rho} \equiv 0$, $\boldsymbol{\Omega}_L = \boldsymbol{\Omega}_{PL} \equiv 0$, and $\dot{\boldsymbol{s}} \equiv 0$. This gives us:

$$mg\boldsymbol{e}_3{}^{\mathrm{T}}\boldsymbol{\Gamma}_L + f_L = 0,\ mg\rho\boldsymbol{e}_3 \times \boldsymbol{\Gamma}_L - \boldsymbol{R}_{PL}\boldsymbol{\tau}_D + \boldsymbol{\tau}_L = 0,\ \boldsymbol{\tau}_D = 0,\ \text{and}\ \boldsymbol{u}_s = 0. \tag{19}$$

These conditions need to be simultaneously satisfied at an equilibrium of the RMP, which leads to $\boldsymbol{\Gamma}_L = \pm\boldsymbol{e}_3$ and $f_L = \mp mg$, while the configuration variables $(\rho, \boldsymbol{R}_L, \boldsymbol{R}_{PL}, \boldsymbol{s})$ are constant at the equilibria, noting that $\boldsymbol{\tau}_D = 0 \Leftrightarrow \boldsymbol{\Omega}_{PL} = 0$. Therefore, instead of disconnected (isolated) equilibrium points, we have two equilibrium manifolds for the RMP for which $\boldsymbol{\Gamma}_L = \pm\boldsymbol{e}_3$. i.e., the leg is along or opposite to the gravity direction, given by $\boldsymbol{e}_3$ in the inertial frame. Therefore the equilibrium manifolds are given by:

$$\mathcal{E}_1 = \big\{(\rho, \boldsymbol{R}_L, \boldsymbol{R}_{PL}, \boldsymbol{s}, \dot{\rho}, \boldsymbol{\Omega}_L, \boldsymbol{\Omega}_{PL}, \dot{\boldsymbol{s}}) \in \mathrm{T}\mathcal{C} : f_L = -mg, \boldsymbol{\Gamma}_L = \boldsymbol{e}_3, \dot{\rho} = 0, \boldsymbol{\Omega}_L = \boldsymbol{\Omega}_{PL} = 0, \dot{\boldsymbol{s}} = 0\big\}, \tag{20}$$

$$\mathcal{E}_2 = \big\{(\rho, \boldsymbol{R}_L, \boldsymbol{R}_{PL}, \boldsymbol{s}, \dot{\rho}, \boldsymbol{\Omega}_L, \boldsymbol{\Omega}_{PL}, \dot{\boldsymbol{s}}) \in \mathrm{T}\mathcal{C} : f_L = mg, \boldsymbol{\Gamma}_L = -\boldsymbol{e}_3, \dot{\rho} = 0, \boldsymbol{\Omega}_L = \boldsymbol{\Omega}_{PL} = 0, \dot{\boldsymbol{s}} = 0\big\}. \tag{21}$$

Since $\boldsymbol{e}_3$ denotes the direction of gravity in the inertial frame, we call $\mathcal{E}_1$ the "hanging equilibrium manifold" and $\mathcal{E}_2$ the "inverted equilibrium manifold". This terminology has been used in prior literature on rigid body and multibody pendulum models [21–24]. The RMP is depicted close to these equilibrium orientations in Fig. 4. For modeling humanoid walking motion, the inverted equilibrium manifold of the RMP and its stabilization is of primary importance. In the following subsection, we look at a simplification of the reaction mass pendulum model with fixed proof masses.

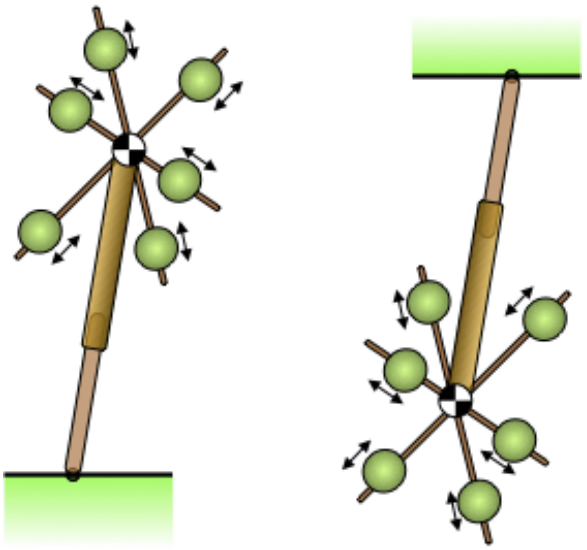

Fig. 4. The RMP is shown close to an inverted orientation in the figure on the left, while the figure on the right shows the RMP close to a hanging orientation.

3.2.4 Stability Properties of the RMP Equilibria

Stability properties of the equilibria (20)-(21) of the RMP are given by the following result, based on linearization of the dynamics about these equilibria.

Proposition 2. *The equilibrium manifold of the RMP system $\mathcal{E}_1$, given by* (20)*, is stable. The equilibrium manifold $\mathcal{E}_2$, given by* (21)*, is unstable.*

Proof: The stability properties of the equilibrium manifolds can be obtained from linearizing the rotational dynamics of the RMP leg in the vicinity of these equilibria. Note that the

linearization of the dynamics for the other degrees of freedom are trivial, as can be seen from the dynamics equations (9), (11) and (12). The linearized rotational dynamics of the RMP leg about the equilibrium manifold $m\boldsymbol{e}_1$ is given by

$$\boldsymbol{J}_L \Delta\ddot{\boldsymbol{\Theta}}_L = mg\rho_e \left(\boldsymbol{e}_3{}^{\times}\right)^2 \Delta\boldsymbol{\Theta}_L, \tag{22}$$

while its linearization about the equilibrium manifold $m\boldsymbol{e}_2$ is given by

$$\boldsymbol{J}_L \Delta\ddot{\boldsymbol{\Theta}}_L = -mg\rho_e \left(\boldsymbol{e}_3{}^{\times}\right)^2 \Delta\boldsymbol{\Theta}_L, \tag{23}$$

where $\Delta\boldsymbol{\Gamma}_L = \boldsymbol{\Gamma}_{L_e} \times \Delta\Theta_L$, $\boldsymbol{\Gamma}_{L_e} = \boldsymbol{e}_3$ for $\mathcal{E}_1$ and $\boldsymbol{\Gamma}_{L_e} = -\boldsymbol{e}_3$ for $\mathcal{E}_2$. Here ρ_e is a constant value of ρ at these equilibrium manifolds; note that the only constraint is for this value to be constant on either of these equilibrium manifolds. The coefficient matrix on the RHS of equation (22) is negative semi-definite, while the coefficient matrix on the RHS of equation (23) is positive semi-definite. Therefore, equation (22) leads to locally Lyapunov stable dynamics at the equilibrium manifold $\mathcal{E}_1$, while equation (23) gives unstable dynamics at the equilibrium manifold $\mathcal{E}_2$. □

3.3 RMP with Fixed Proof Masses

When the proof mass positions are fixed in the proof mass assembly, the vector $\boldsymbol{s}$ is constant. This reduces the full dynamical model of the RMP, which has ten degrees of freedom (DOFs) as provided by equations (1)-(3) and (9)-(12), to one that has only seven degrees of freedom. The kinematic relations (1)-(3) still hold for this reduced model, since the DOFs associated with these relations (ρ, $\boldsymbol{\Omega}_L$ and $\boldsymbol{\Omega}_{PL}$) are present in this reduced model. The configuration space of this reduced RMP system is $\mathcal{P} = [0, r] \times \mathrm{SO}(3) \times \mathrm{SO}(3) \subset \mathcal{C}$. Like the complete RMP model, this reduced model with fixed proof masses is also *underactuated*, with four actuated DOFs: one for the length of the RMP leg varied by the prismatic actuator, and the three rotational DOFs of the RMP leg actuated by the torque applied at the ankle joint. The dynamics equations of motion are obtained by restricting $\boldsymbol{s}$ to be constant in the full dynamics model given by Proposition 1. This is stated below as Corollary 1.

Corollary 1. *The reduced reaction mass pendulum model depicted in Figure 2, with fixed proof mass positions in the proof mass assembly, has the following dynamics equations:*

$$m\ddot{\rho} = -m\rho\boldsymbol{\Omega}_L{}^{\mathrm{T}} \left(\boldsymbol{e}_3{}^{\times}\right)^2 \boldsymbol{\Omega}_L + mg\boldsymbol{e}_3{}^{\mathrm{T}}\boldsymbol{\Gamma}_L + f_L, \tag{24}$$

$$\begin{aligned}\boldsymbol{J}_L(\rho)\dot{\boldsymbol{\Omega}}_L = {} & \boldsymbol{J}_L(\rho)\boldsymbol{\Omega}_L \times \boldsymbol{\Omega}_L + 2m\rho\dot{\rho}\left(\boldsymbol{e}_3{}^{\times}\right)^2\boldsymbol{\Omega}_L + \\ & mg\rho\boldsymbol{e}_3 \times \boldsymbol{\Gamma}_L - \boldsymbol{R}_{PL}\boldsymbol{\tau}_D + \boldsymbol{\tau}_L,\end{aligned} \tag{25}$$

$$\boldsymbol{J}_P\dot{\boldsymbol{\Omega}}_P = \boldsymbol{J}_P\boldsymbol{\Omega}_P \times \boldsymbol{\Omega}_P + \boldsymbol{\tau}_D, \tag{26}$$

$$\text{where } \boldsymbol{J}_P = \boldsymbol{J}_{P_0} - 2m_p\sum_{i=1}^{3} s_i^2(\boldsymbol{e}_i{}^{\times})^2. \tag{27}$$

Here $\boldsymbol{s} = [s_1 \;\; s_2 \;\; s_3]^{\mathrm{T}}$ is the constant vector of positions of the proof masses in the coordinate frame fixed to the proof mass assembly.

The proof of this result follows immediately from Proposition 1 by constraining $\boldsymbol{s}$ to be constant.

4 Stabilization of Inverted Equilibrium Manifold of RMP

The complete dynamics of the RMP model as given by Proposition 1 is clearly underactuated, with ten DOFs and seven control inputs. In this section, a nonlinear control scheme for stabilizing the inverted equilibrium manifold $m\boldsymbol{e}_2$ of the RMP is presented, along with proof of its stability properties. We propose a control law that stabilizes the motion of the RMP to an inverted equilibrium with a desired leg length and desired positions of the proof mass actuators. The control law is stated in the following theorem, which is one of the two main results of this article.

Theorem 1. *Consider the RMP system whose dynamics model is given by equations* (1)-(3) *and equations* (9)-(12). *Let $\Phi : \mathbb{R}^+ \to \mathbb{R}^+$ be a $\mathcal{C}^2$ function that satisfies $\Phi(0) = 0$ and $\Phi'(x) > 0$ for all $x \in \mathbb{R}^+$. Furthermore, let $\Phi'(\cdot) \leq \alpha(\cdot)$ where $\alpha(\cdot)$ is a Class-$\mathcal{K}$ function [31]. Let $\gamma > 0$ and $k > 0$ be positive scalar control gains, $\boldsymbol{G}$, $\boldsymbol{L}_\Omega$ and $\boldsymbol{P}$ be 3×3 positive definite gain matrices and let $\boldsymbol{A} = \mathrm{diag}\{a_1, a_2, a_3\}$ where $a_3 > a_2 > a_1 > 0$. Let $\boldsymbol{E}_2 = \mathrm{diag}\{-1, 1, -1\} \in \mathcal{E}_2$ be the desired final attitude of the RMP leg. Then the control laws*

$$f_L = -mg\boldsymbol{e}_3{}^{\mathrm{T}}\boldsymbol{\Gamma}_L - k(\rho - \rho_e) - \gamma\dot{\rho}, \tag{28}$$

$$u_s = -\boldsymbol{P}(s - s_e) - \boldsymbol{G}\dot{\boldsymbol{s}}, \tag{29}$$

$$\boldsymbol{\tau}_L = mg\rho\boldsymbol{\Gamma}_L \times \boldsymbol{e}_3 - \boldsymbol{L}_\Omega\boldsymbol{\Omega}_L - \Phi'\big(\mathrm{trace}(\boldsymbol{A} - \boldsymbol{A}\boldsymbol{Q}_L)\big)\boldsymbol{S}(\boldsymbol{Q}_L), \tag{30}$$

where $\boldsymbol{Q}_L = \boldsymbol{E}_2{}^{\mathrm{T}}\boldsymbol{R}_L$ and $\boldsymbol{S}(\boldsymbol{Q}_L) = \sum_{i=1}^{3} a_i\boldsymbol{Q}_L^{\mathrm{T}}\boldsymbol{e}_i \times \boldsymbol{e}_i$,

asymptotically stabilize the set of equilibria defined by

$$\begin{aligned}\mathcal{S}_L = \big\{ & \big(\rho, \boldsymbol{R}_L, \boldsymbol{R}_{PL}, \boldsymbol{s}, \dot{\rho}, \boldsymbol{\Omega}_L, \boldsymbol{\Omega}_{PL}, \dot{\boldsymbol{s}}\big) : \rho = \rho_e, \boldsymbol{R}_L = \boldsymbol{E}_2, \boldsymbol{s} = \boldsymbol{s}_e, \\ & \dot{\rho} = 0, \boldsymbol{\Omega}_L = 0, \boldsymbol{\Omega}_{PL} = 0, \dot{\boldsymbol{s}} = 0\big\} \subset \mathcal{E}_2.\end{aligned} \tag{31}$$

Proof: The proof of this result is obtained using generalizations of Lyapunov's direct method and LaSalle's invariance principle. The configuration space $\mathcal{C}$ has the compact, non-contractible manifold $\mathrm{SO}(3)$ as a component. Moreover, the desired set we want to stabilize, $\mathcal{S}_L$, requires stabilization of the RMP leg attitude $\boldsymbol{R}_L \in \mathrm{SO}(3)$ to a desired attitude given by $\boldsymbol{R}_L = \boldsymbol{E}_2$. Since any particular configuration on $\mathrm{SO}(3)$, which is the configuration space for rigid body attitude systems, cannot be globally asymptotically stabilized using continuous feedback (see [32–35]), we obtain almost global stabilization of the desired set $\mathcal{S}_L$. Moreover, for continuous stabilization of the leg attitude, we need a Morse function that generalizes the concept of a Lyapunov function to a nonlinear state space [36]. The candidate Morse-Lyapunov function V for stabilizing the motion of the RMP to the set $\mathcal{S}_L$ is obtained as a sum of two functions: (a) V_L, which depends on

the motion of the leg, and (b) V_P, which depends on the motion of the RMP's PMA assembly (RMP body). The function $V_L : \mathcal{C} \times \mathbb{R}^{10} \to \mathbb{R}^+$ that depends on the motion of the leg is defined by

$$V_L(\rho, \boldsymbol{R}_L, \dot{\rho}, \boldsymbol{\Omega}_L) = \frac{1}{2} m \dot{\rho}^2 + \frac{1}{2} \boldsymbol{\Omega}_L{}^{\mathrm{T}} \boldsymbol{J}_L(\rho) \boldsymbol{\Omega}_L + \frac{1}{2} k (\rho - \rho_e)^2 + \Phi\big(\mathrm{trace}(\boldsymbol{A} - \boldsymbol{A}\boldsymbol{Q}_L)\big). \tag{32}$$

The time derivative of this component of the Lyapunov function is given by

$$\dot{V}_L = m \dot{\rho} \ddot{\rho} + \boldsymbol{\Omega}_L{}^{\mathrm{T}} \boldsymbol{J}_L(\rho) \dot{\boldsymbol{\Omega}}_L - m \rho \dot{\rho} \boldsymbol{\Omega}_L{}^{\mathrm{T}} \big(\boldsymbol{e}_3{}^{\times}\big)^2 \boldsymbol{\Omega}_L + k(\rho - \rho_e)\dot{\rho} + \Phi'\big(\mathrm{trace}(\boldsymbol{A} - \boldsymbol{A}\boldsymbol{Q}_L)\big) \boldsymbol{\Omega}_L{}^{\mathrm{T}} \boldsymbol{S}(\boldsymbol{Q}_L),$$

where the last term in the second row above is the time derivative of $\Phi\big(\mathrm{trace}(\boldsymbol{A} - \boldsymbol{A}\boldsymbol{Q}_L)\big)$ and $\Phi'(x)$ denotes the derivative of $\Phi(x)$ with respect to x. Substituting the dynamics equations (9)-(12) into this expression for $\dot{V}_L$, we get

$$\dot{V}_L = \dot{\rho}\big[m g \boldsymbol{e}_3{}^{\mathrm{T}} \boldsymbol{\Gamma}_L + f_L + k(\rho - \rho_e)\big] + \boldsymbol{\Omega}_L{}^{\mathrm{T}}\big[m g \rho \boldsymbol{e}_3 \times \boldsymbol{\Gamma}_L + \Phi'\big(\mathrm{trace}(\boldsymbol{A} - \boldsymbol{A}\boldsymbol{Q}_L)\big) \boldsymbol{S}(\boldsymbol{Q}_L) - \boldsymbol{R}_{PL} \boldsymbol{\tau}_D\big].$$

Further substitution of the control laws (28)-(30) and $\boldsymbol{\tau}_D = -\boldsymbol{D}\boldsymbol{\Omega}_{PL}$ into this last expression for $\dot{V}_L$ gives us

$$\dot{V}_L = -\gamma \dot{\rho}^2 - \boldsymbol{\Omega}_L{}^{\mathrm{T}} \boldsymbol{L}_{\Omega} \boldsymbol{\Omega}_L + \boldsymbol{\Omega}_L{}^{\mathrm{T}} \boldsymbol{R}_{PL} \boldsymbol{D} \boldsymbol{\Omega}_{PL}, \tag{33}$$

for the closed-loop system given by equations (1)-(3) and (9)-(12), along with the control laws (28)-(30).

Now we consider the component of the Lyapunov function that depends on the motion of the PMA assembly; this component is defined by

$$V_P(\boldsymbol{\Omega}_P, \boldsymbol{s}, \dot{\boldsymbol{s}}) = \frac{1}{2} \boldsymbol{\Omega}_P{}^{\mathrm{T}} \boldsymbol{J}_P(\boldsymbol{s}) \boldsymbol{\Omega}_P + m_p \dot{\boldsymbol{s}}^{\mathrm{T}} \dot{\boldsymbol{s}} + \frac{1}{2} \boldsymbol{z}^{\mathrm{T}} \boldsymbol{P} \boldsymbol{z}, \tag{34}$$

where $\boldsymbol{z} = \boldsymbol{s} - \boldsymbol{s}_e$. The time derivative of this function is given by

$$\dot{V}_P = \boldsymbol{\Omega}_P{}^{\mathrm{T}} \boldsymbol{J}_P(\boldsymbol{s}) \dot{\boldsymbol{\Omega}}_P + \frac{1}{2} \boldsymbol{\Omega}_P{}^{\mathrm{T}} \boldsymbol{N}(s, \dot{\boldsymbol{s}}) \boldsymbol{\Omega}_P + 2 m_p \dot{\boldsymbol{s}}^{\mathrm{T}} \ddot{\boldsymbol{s}} + \boldsymbol{z}^{\mathrm{T}} \boldsymbol{P} \dot{\boldsymbol{s}}. \tag{35}$$

Substituting the dynamics equations (11)-(12) into equation (35), we obtain the time derivative of V_P along the dynamics of the PMA assembly as

$$\dot{V}_P = -\frac{1}{2} \boldsymbol{\Omega}_P{}^{\mathrm{T}} \boldsymbol{N}(\boldsymbol{s}, \dot{\boldsymbol{s}}) \boldsymbol{\Omega}_P - \boldsymbol{\Omega}_P{}^{\mathrm{T}} \boldsymbol{D} \boldsymbol{\Omega}_{PL} + \dot{\boldsymbol{s}}^{\mathrm{T}} \big\{\boldsymbol{L}(\boldsymbol{s}, \boldsymbol{\Omega}_P) + \boldsymbol{u}_s + \boldsymbol{P}\boldsymbol{z}\big\}. \tag{36}$$

From the expressions for $N(\boldsymbol{s}, \dot{\boldsymbol{s}})$ and $L(\boldsymbol{s}, \boldsymbol{\Omega}_P)$ given in Proposition 1, one can verify that

$$\dot{\boldsymbol{s}}^{\mathrm{T}} \boldsymbol{L}(\boldsymbol{s}, \boldsymbol{\Omega}_P) = \frac{1}{2} \boldsymbol{\Omega}_P{}^{\mathrm{T}} \boldsymbol{N}(\boldsymbol{s}, \dot{\boldsymbol{s}}) \boldsymbol{\Omega}_P.$$

Therefore the above expression for $\dot{V}_P$ simplifies to

$$\dot{V}_P = -\boldsymbol{\Omega}_P{}^{\mathrm{T}} \boldsymbol{D} \boldsymbol{\Omega}_{PL} + \dot{\boldsymbol{s}}^{\mathrm{T}} \big\{\boldsymbol{u}_s + \boldsymbol{P}\boldsymbol{z}\big\}. \tag{37}$$

Now substituting the control law (29) into the above expression, we get

$$\dot{V}_P = -\boldsymbol{\Omega}_P{}^{\mathrm{T}} \boldsymbol{D} \boldsymbol{\Omega}_{PL} - \dot{\boldsymbol{s}}^{\mathrm{T}} \boldsymbol{G} \dot{\boldsymbol{s}}. \tag{38}$$

We combine V_L and V_P to form the Morse-Lyapunov function $V = V_L + V_P$. Combining the expressions for $\dot{V}_L$ and $\dot{V}_P$ from (33) and (38) respectively, we obtain

$$\dot{V} = \dot{V}_L + \dot{V}_P = -\gamma \dot{\rho}^2 - \boldsymbol{\Omega}_L{}^{\mathrm{T}} \boldsymbol{L}_{\Omega} \boldsymbol{\Omega}_L - \boldsymbol{\Omega}_{PL}{}^{\mathrm{T}} \boldsymbol{D} \boldsymbol{\Omega}_{PL} - \dot{\boldsymbol{s}}^{\mathrm{T}} \boldsymbol{G} \dot{\boldsymbol{s}}. \tag{39}$$

Therefore, $\dot{V}$ is negative semi-definite in the states for the closed-loop system given by equations (1)-(3) and (9)-(12), along with the control laws (28)-(30). Moreover, from the expression (39) for $\dot{V}$, we see that $\dot{\rho} \to 0, \boldsymbol{\Omega}_L \to 0, \boldsymbol{\Omega}_{PL} \to 0$ (and hence $\boldsymbol{\Omega}_P = \boldsymbol{\Omega}_{PL} + \boldsymbol{R}_{PL}{}^{\mathrm{T}} \boldsymbol{\Omega}_L \to 0$), and $\dot{\boldsymbol{s}} \to 0$ as time $t \to \infty$. When the closed-loop system is restricted to the set $\dot{V}^{-1}(0)$, we get

$$-k(\rho - \rho_e) = 0, \; -\boldsymbol{P}(\boldsymbol{s} - \boldsymbol{s}_e) = 0, \quad \text{and} \; -\Phi'\big(\mathrm{trace}(\boldsymbol{A} - \boldsymbol{A}\boldsymbol{Q}_L)\big) \boldsymbol{S}(\boldsymbol{Q}_L) = 0, \tag{40}$$

which characterizes the largest invariant set $\mathbf{I} \subset \dot{V}^{-1}(0) \subset \mathcal{C} \times \mathbb{R}^{10}$. The last condition in (40) gives the set of critical points $\mathcal{E}_c$ of $\Phi\big(\mathrm{trace}(\boldsymbol{A} - \boldsymbol{A}\boldsymbol{Q}_L)\big)$:

$$\mathcal{E}_c = \big\{\boldsymbol{I}, \mathrm{diag}\{1,-1,-1\}, \mathrm{diag}\{-1,1,-1\}, \mathrm{diag}\{-1,-1,1\}\big\},$$

where $\boldsymbol{I}$ denotes the 3×3 identity matrix. Within this set of critical points, it can be shown, as in [33–35], that $\boldsymbol{Q}_L = \boldsymbol{I}$ is the minimum, while the other points ($Q_L \in \mathcal{E}_c \setminus \boldsymbol{I}$) are non-degenerate critical points. Therefore, as $\dot{V} \leq 0$ along the trajectories of the feedback system, the only stable subset of the invariant set is $\mathcal{S}_L \subset \mathbf{I}$. The other critical points (corresponding to leg attitude $Q_L \in \mathcal{E}_c \setminus \boldsymbol{I}$) are unstable for the feedback system, although they may have stable manifolds. Therefore, except for those trajectories that start on the stable manifolds of $\mathbf{I} \setminus \mathcal{S}_L$, all other trajectories in $\mathcal{C} \times \mathbb{R}^{10}$ converge asymptotically to $\mathcal{S}_L$. Since the largest invariant set $\mathbf{I}$ of the feedback system is itself of zero measure in the state space $\mathcal{C} \times \mathbb{R}^{10}$, this means that the set $\mathcal{S}_L$ is asymptotically stable and its domain of attraction is almost global. □

The above result gives control laws for stabilizing the set $\mathcal{S}_L$, where the leg of the RMP is in an "inverted orientation". Note that the set $\mathcal{S}_L$ is a subset of $\mathcal{E}_2$, the inverted

equilibrium manifold of the RMP. However, the final attitude of the RMP body (PMA assembly) is not specified in the set $\mathcal{S}_L$. Therefore, all that can be concluded is that the RMP body will come to rest at some final attitude. The passive (viscous) damping at the hip joint serves to damp out the rotational motion of the RMP body.

5 Numerical Simulation for Stabilization of Inverted Equilibrium of RMP

Here we present some numerical simulation results of applying the control scheme described earlier in this section. The mass and inertia properties of the RMP are chosen to be similar to that of a NAO robot, and are given as follows

$$m_L = 0.882 \text{ kg}, \ \boldsymbol{J}_{L_0} = 0.5\big(\text{diag}\{0.98, 0.91, 0.63\}\big) \text{ kg-m}^2,$$
$$m_P = 0.32 \text{ kg}, \ \boldsymbol{J}_{P_0} = \begin{bmatrix} 0.2126 & 0.0004 & -0.0002 \\ 0.0004 & 0.2042 & 0.0010 \\ -0.0002 & 0.0010 & 0.2246 \end{bmatrix} \text{ kg-m}^2.$$

The initial vector of positions for the three pairs of proof masses is given by

$$\boldsymbol{s} = 1.47\big([0.035 \ \ 0.025 \ \ 0.028]^{\mathrm{T}}\big) \text{ m}.$$

The initial leg length, and initial attitudes of the leg and body (PMA assembly) of the RMP are

$$\rho(0) = 0.41 \text{ m}, \ \boldsymbol{R}_L(0) = \begin{bmatrix} -0.4767 & -0.8325 & -0.2823 \\ -0.4966 & 0.5201 & -0.6949 \\ 0.7253 & -0.1911 & -0.6613 \end{bmatrix},$$
$$\boldsymbol{R}_{PL}(0) = \begin{bmatrix} 0.9493 & -0.2463 & -0.1956 \\ 0.1956 & 0.9493 & -0.2463 \\ 0.2463 & 0.1956 & 0.9493 \end{bmatrix}.$$

The initial leg attitude $\boldsymbol{R}_L(0)$ is such that its longitudinal axis given by $\boldsymbol{\Gamma}_L(0)$ makes an angle of 2.2934 radians$= 131.40^\circ$ to the direction of uniform gravity (inertial z-axis), while the initial attitude of the PMA assembly is obtained by a rotation of an angle of $22.5^\circ = \frac{\pi}{8}$ radians about the axis $[1 \ \ -1 \ \ 1]^{\mathrm{T}}/\sqrt{3}$ in the leg-fixed coordinate frame.

The desired set of motions to be stabilized is given by $\mathcal{S}_L$ in equation (31) with $\rho_e = 0.35$ m and

$$\boldsymbol{s}_e = [0.0735 \ \ 0.0525 \ \ 0.0588]^{\mathrm{T}} \text{ m}.$$

The control gain values chosen for this simulation are:

$$k = 0.91, \ \gamma = 1.4, \ \boldsymbol{L}_\Omega = 0.98\big(\text{diag}\{2, 3, 4\}\big),$$
$$\boldsymbol{A} = \text{diag}\{1.2, 1.5, 1.8\}, \ \boldsymbol{P} = \begin{bmatrix} 1.1 & -0.2 & 0.1 \\ -0.2 & 1.2 & 0.3 \\ 0.1 & 0.3 & 1.3 \end{bmatrix},$$
and $\boldsymbol{G} = 0.42\boldsymbol{I}$.

The viscous damping coefficient matrix for the "hip joint" supporting the PMA assembly is

$$\boldsymbol{D} = 0.03\boldsymbol{I}.$$

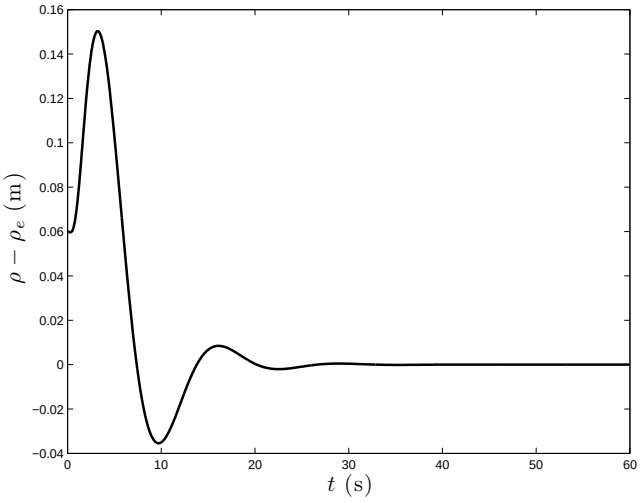

Fig. 5. Time plot of $\rho - \rho_e$ for the RMP system with the feedback control scheme of Theorem 1. Here $\rho_e = 0.35$ m and the initial vlue of ρ is 0.41 m.

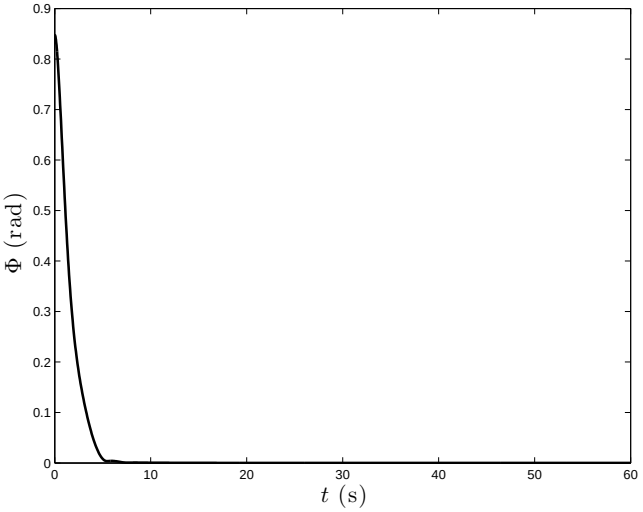

Fig. 6. Time plot of the angle Φ between the reduced attitude $\boldsymbol{\Gamma}_L = \boldsymbol{R}_L{}^{\mathrm{T}}\boldsymbol{e}_3$ of the RMP leg and the opposite direction to uniform gravity $-\boldsymbol{e}_3$, for the RMP system with the feedback control scheme of Theorem 1. Here $\Phi = 48.6^\circ$ at the start of the simulation and the final desired value of Φ is 0°.

We numerically simulate the dynamics of the feedback system over a period of one minute (60 seconds). Figure 5 gives the time plot of $\Delta\rho = \rho - \rho_e$ for the feedback system. Figure 6 gives the time plot of the angle Φ between the $\boldsymbol{\Gamma}_L$ vector and the direction opposite to uniform gravity, i.e., $\cos\Phi = -\boldsymbol{e}_3{}^{\mathrm{T}}\boldsymbol{\Gamma}_L = -\boldsymbol{e}_3{}^{\mathrm{T}}\boldsymbol{R}_L{}^{\mathrm{T}}\boldsymbol{e}_3$. In [21–24,32], $\boldsymbol{\Gamma}_L$ is referred to as the *reduced attitude* vector of the rigid or multibody pendulum system. Note that since the leg's longitudinal axis direction $\boldsymbol{\Gamma}_L$ initially makes an angle of 131.4° to the gravity direction, the initial angle made with the desired axis direction for the equilibrium set $\mathcal{S}_L$ is $180^\circ - 131.4^\circ = 48.6^\circ$. Both the configuration variables ρ and $\boldsymbol{\Gamma}_L$ are seen to con-

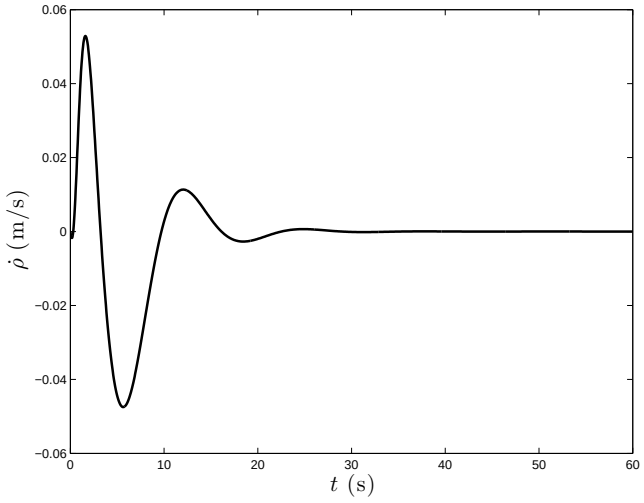

Fig. 7. Time plot of the velocity $\dot{\rho}$ of extension or retraction of the RMP leg, for the RMP system with the feedback control scheme of Theorem 1. Both the initial and the final desired value of $\dot{\rho}$ is 0 m/s.

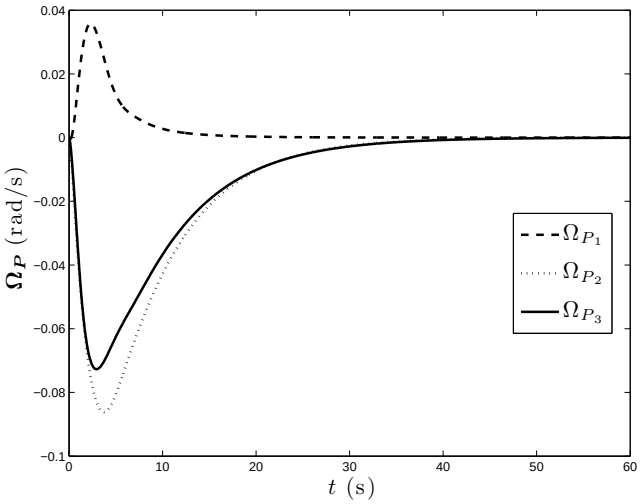

Fig. 9. Time plots of the components of the angular velocity $\boldsymbol{\Omega}_P$ of the RMP PMA assembly, for the RMP system with the feedback control scheme of Theorem 1.

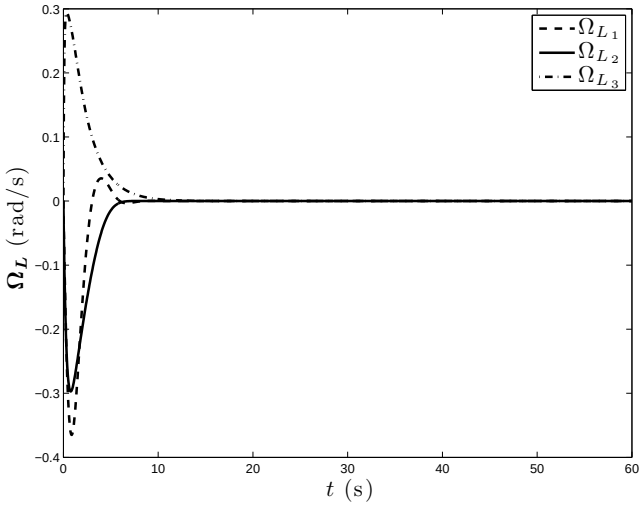

Fig. 8. Time plots of the components of the angular velocity $\boldsymbol{\Omega}_L$ of the RMP leg, for the RMP system with the feedback control scheme of Theorem 1. Both the initial and the final desired values of these components are 0 rad/s.

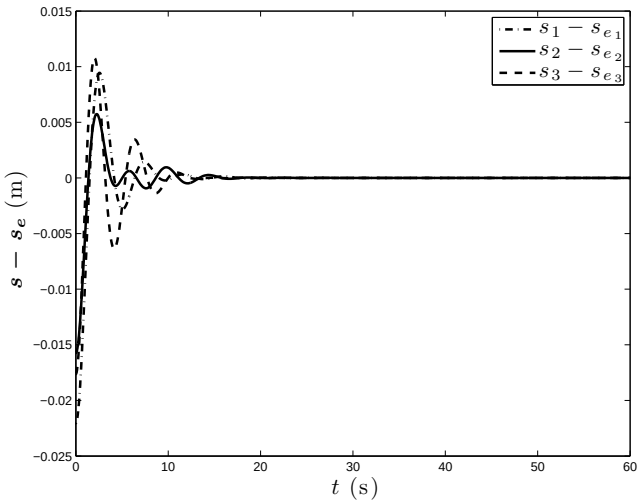

Fig. 10. Time plots of the components of the vector difference of PMA locations $\boldsymbol{s}$ and desired locations $\boldsymbol{s}_e$, for the RMP system with the feedback control scheme of Theorem 1.

verge to the desired final values during the time period of this simulation.

Figure 7 gives the time evolution of the velocity variable $\dot{\rho}$, which is the speed of extension of retraction of the leg of the RMP due to the prismatic actuator. Figure 8 gives the time plots of the components of the angular velocity vector $\boldsymbol{\Omega}_L$ of the RMP leg over the simulation period. It is to be noted that these velocity states are seen to asymptotically converge to zero over the time period of simulation (120 s). Therefore, from figures 5-8, we see that the RMP leg is stabilized to an "inverted" attitude with its longitudinal axis opposite the direction of gravity, and its length stabilized to the desired value by the prismatic force actuator on the leg.

The time plot of the angular velocity $\boldsymbol{\Omega}_P$ of the PMA assembly (RMP body) during this simulation period, is given in Figure 9. As noted in the earlier section, the PMA assembly comes to a rest attitude as the angular velocity $\boldsymbol{\Omega}_P$ converges to the zero vector when the motion states converge asymptotically to the inverted equilibrium set $\mathcal{S}_L$. Figure 10 gives the time plots of the components of the vector difference of PMA locations $\boldsymbol{s}$ and the desired final PMA location vector $\boldsymbol{s}_e$ over the simulated time duration. The components of $\boldsymbol{s} - \boldsymbol{s}_e$ are seen to converge to zero, as predicted by Theorem 1 for the RMP feedback controlled system.

Finally, time plots of the components of the control torque vector $\boldsymbol{\tau}_L$ applied to the RMP leg at the ankle joint, are given in Figure 11. These components are also seen to

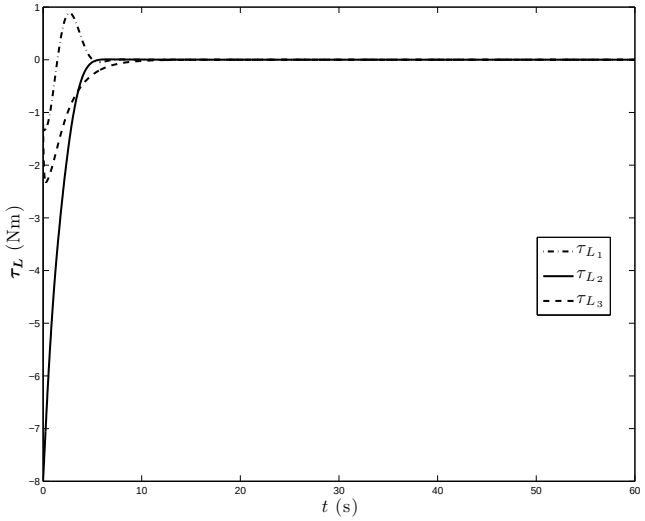

Fig. 11. Time plots of the components of the control torque vector $\boldsymbol{\tau}_L$ applied at the ankle joint of the RMP with the feedback control scheme of Theorem 1.

converge to zero over the simulated time duration, since the feedback system converges to an equilibrium state. The large initial component of $\boldsymbol{\tau}_L$ is due to the relatively large initial angle (48.6°) between the longitudinal axis of the RMP leg and the desired upright or "inverted" equilibrium orientation of this axis. The initial transient behavior of $\boldsymbol{\tau}_L$ can be modified by changing the control gains L_Ω and A in control law (30). As remarked earlier, in the case that the spherical ankle joint has two degrees of freedom and does not allow rotation along the leg's longitudinal axis, the third component of $\boldsymbol{\tau}_L$ would be a constraint torque that constrains the third component of $\boldsymbol{\Omega}_L$ to be zero.

6 Conclusions

We have introduced the reaction mass pendulum (RMP) as an underactuated 3D multibody system with a variable inertia, and analyzed the dynamics and stabilization of inverted orientations of the RMP. The RMP could be used as a reduced order model of a humanoid robot, and in this role, the RMP is an instantaneous capture of the 3D aggregate kinematics and inertia of the humanoid. The conceptual realization of the RMP consists of a variable length leg and a proof mass assembly (PMA) with three pairs of proof masses that are actuated to move in a symmetric fashion along three mutually perpendicular tracks attached to a spherical joint. The PMA can freely rotate about this spherical joint ("hip joint") that connects it to the RMP leg, with passive (viscous) damping present at this joint. The RMP leg is actuated by a torque applied at another spherical joint (the "ankle joint") connecting the base of the leg to the ground contact point (center of pressure), and a prismatic actuator that varies the length of the leg. The RMP model is an enhancement of existing inverted pendulum humanoid models that contain only a point mass, and is also a mechanical realization of a 3D multibody system with variable rotational inertia. In this work, we derived the dynamics equations of motion using a global representation of the state of this multibody RMP model. The equilibrium configurations of the RMP are shown to lie on two disjoint equilibrium manifolds, which we call the hanging equilibrium manifold and the inverted equilibrium manifold. Stabilization of the inverted equilibrium manifold is of interest for modeling humanoid motion. We also obtained control schemes that asymptotically stabilize an inverted ("upright") equilibrium, where the longitudinal axis of the leg is aligned opposite to direction of uniform gravity, the length of the RMP leg is a desired value, the proof mass assembly comes to rest with zero angular velocity, and the proof mass actuator pairs reach desired positions. The domain of attraction of this feedback stabilization scheme is shown to be almost global in the state space. A future extension of this work will consider tracking of desired motions of the RMP using geometric mechanics-based feedback control.

Acknowledgements

The authors wish to thank the anonymous reviewers whose feedback helped in improving this manuscript.

References

[1] Shiriaev, A. S., Ludvigsen, H., and Egeland, O., 2004. "Swinging up the spherical pendulum via stabilization of its first integrals". *Automatica,* **40**(1), pp. 73–85.

[2] Furuta, K., 2003, Maui, Hawaii. "Control of pendulum: From super mechano-system to human adaptive mechatronics". In IEEE Conference on Decision and Control, pp. 1498–1507.

[3] Astrom, K. J., and Furuta, K., 1996. "Swinging-up a pendulum by energy control". In Proceedings of the IFAC Congress, Vol. E, pp. 37–42.

[4] Kajita, S., and Tani, K., 1991. "Study of dynamic biped locomotion on rugged terrain". In IEEE International Conference on Robotics and Automation (ICRA), pp. 1405–1411.

[5] Kajita, S., Kanehiro, F., Kaneko, K., Yokoi, K., and Hirukawa, H., 2001, Maui, Hawaii. "The 3D linear inverted pendulum model: A simple modeling for a biped walking pattern generator". In IEEE/RSJ International Conference on Intelligent Robots and Systems (IROS), pp. 239–246.

[6] Kajita, S., Kanehiro, F., Kaneko, K., Fujiwara, K., Harada, K., Yokoi, K., and Hirukawa, H., 2003, Taipei, Taiwan. "Biped walking pattern generation by using preview control of zero-moment point". In IEEE International Conference on Robotics and Automation (ICRA), pp. 1620–1626.

[7] Sugihara, T., and Nakamura, Y., 2003, Germany. "Variable impedant inverted pendulum model control for a seamless contact phase transition on humanoid robot". In IEEE International Conference on Humanoid Robots (Humanoids2003), pp. 0–0.

[8] Altendorfer, R., Saranli, U., Komsuoglu, H., Koditschek, D., Brown, H. B., Buehler, M., Moore,

N., McMordie, D., and Full, R., 2001. "Evidence for spring loaded inverted pendulum running in a hexapod robot". In *Experimental Robotics VII*, D. Rus and S. Singh, eds. Springer-Verlag, pp. 291 – 302.

[9] Komura, T., Leung, H., Kudoh, S., and Kuffner, J., 2005, Barcelona, Spain. "A feedback controller for biped humanoids that can counteract large perturbations during gait". In IEEE International Conference on Robotics and Automation (ICRA), pp. 2001–2007.

[10] Komura, T., Nagano, A., Leung, H., and Shinagawa, Y., 2005, September. "Simulating pathological gait using the enhanced linear inverted pendulum model". *IEEE Transactions on Biomedical Engineering,* **52**(9), pp. 1502–1513.

[11] Kuo, A., 2007. "The six determinants of gait and the inverted pendulum analogy: A dynamic walking perspective". *Human Movement Science,* **26**(4), pp. 617–656.

[12] Dutta, A., and Goswami, A., 2010, Providence, Rhode Island, USA. "Human postural model that captures rotational inertia,". In American Society of Biomechanics.

[13] Abdallah, M., and Goswami, A., 2005, Barcelona, Spain. "A biomechanically motivated two-phase strategy for biped robot upright balance control". In IEEE International Conference on Robotics and Automation (ICRA), pp. 3707–3713.

[14] Herr, H., and Popovic, M., 2008. "Angular momentum in human walking". *The Journal of Experimental Biology,* **211**, pp. 467–481.

[15] Hofmann, A., 2006. "Robust execution of biped walking tasks from biomechanical principles". PhD thesis, MIT, AI Lab.

[16] Kajita, S., Kanehiro, F., Kaneko, K., Fujiwara, K., Harada, K., Yokoi, K., and Hirukawa, H., 2003, Las Vegas, NV, USA. "Resolved momentum control: humanoid motion planning based on the linear and angular momentum". In IEEE/RSJ International Conference on Intelligent Robots and Systems (IROS), Vol. 2, pp. 1644–1650.

[17] Vermeulen, J., Verrelst, B., Vanderborght, B., Lefeber, D., and Guillaume, P., 2006. "Trajectory planning for the walking biped "lucy"". *International Journal of Robotics Research,* **25**(9), pp. 867–887.

[18] Westervelt, E., Grizzle, J. W., Chevallereau, C., Choi, J. O., and Morris, B., 2007. *Feedback Control of Dynamic Bipedal Robot Locomotion*. CRC Press, Boca Raton, FL.

[19] Lee, S.-H., and Goswami, A., 2007, Rome, Italy. "Reaction mass pendulum (RMP): An explicit model for centroidal angular momentum of humanoid robots". In IEEE International Conference on Robotics and Automation (ICRA), pp. 4667–4672.

[20] Hernandez-Garduno, A., Lawson, J. L., and Marsden, J. E., 2004. Relative equilibria for the generalized rigid body. Tech. rep., Mathematics Faculty Research Paper. Trinity University.

[21] Shen, J., Sanyal, A. K., Chaturvedi, N. A., Bernstein, D. S., and McClamroch, N. H., 2004, Nassau, Bahamas. "Dynamics and control of a 3D pendulum". In IEEE Conference on Decision and Control, pp. 323–328.

[22] Shen, J., Sanyal, A. K., and McClamroch, N. H., 2003. "Asymptotic stability of multibody attitude systems". In *Stability and Control of Dynamical Systems with Applications*, D. Liu and J. Antsaklis, eds. Birkhauser, pp. 291–302.

[23] Chaturvedi, N. A., Bacconi, F., Sanyal, A. K., Bernstein, D. S., and McClamroch, N. H., 2005, Portland, Oregon. "Stabilization of a 3D rigid pendulum". In American Control Conference, pp. 3030–3035.

[24] Chaturvedi, N. A., and McClamroch, N. H., 2006, San Diego, CA. "Global stabilization of an inverted 3D pendulum including control saturation effects". In IEEE Conference on Decision and Control, pp. 6488–6493.

[25] Astrom, K., Block, A., and Spong, M., 2001. *The Reaction Wheel Pendulum*. Downloadable from: http://decision.csl.uiuc.edu/ spong/main.htm.

[26] Sanyal, A. K., and Goswami, A., 2011, Arlington, VA, USA. "Dynamics and control of the reaction mass pendulum (RMP) as a 3D multibody system: Application to humanoid modeling". In ASME Dynamic Systems and Control Conference, pp. 589–596.

[27] Goldstein, H., 1980. *Classical Mechanics*, 2 ed. Addison-Wesley, Reading, MA.

[28] Bloch, A. M., 2003. *Nonholonomic Mechanics and Control*. No. 24 in Interdisciplinary Texts in Mathematics. Springer Verlag.

[29] Abraham, R., and Marsden, J. E., 1978. *Foundations of Mechanics*, 2 ed. Benjamin/Cummings Publishing Company.

[30] Shen, J., 2002. "Nonlinear control of multibody systems with symmetries via shape change". PhD thesis, University of Michigan, Ann Arbor, MI, July.

[31] Khalil, H. K., 1995. *Nonlinear Systems*, 2 ed. Prentice Hall, Englewood Cliffs, NJ.

[32] Chaturvedi, N. A., McClamroch, N. H., and Bernstein, D. S., 2009. "Asymptotic smooth stabilization of the inverted 3D pendulum". *IEEE Transactions on Automatic Control,* **54**(6), June, pp. 1204–1215.

[33] Sanyal, A. K., and Chaturvedi, N. A., 2008, Honolulu. "Almost global robust attitude tracking control of spacecraft in gravity". In AIAA Guidance, Navigation and Control Conference, pp. AIAA–2008–6979.

[34] Sanyal, A. K., Fosbury, A., Chaturvedi, N. A., and Bernstein, D. S., 2009. "Inertia-free spacecraft attitude trajectory tracking with disturbance rejection and almost global stabilization". *AIAA Journal of Guidance, Control and Dynamics,* **32**(2), Feb, pp. 1167–1178.

[35] Chaturvedi, N. A., Sanyal, A. K., and McClamroch, N. H., 2011. "Rigid-Body Attitude Control: Using rotation matrices for continuous, singularity-free control laws". *IEEE Control Systems Magazine,* **31**(3), June, pp. 30–51.

[36] Milnor, J., 1963. *Morse Theory*. Princeton University Press, Princeton, NJ.